

INTEGRAL FIELD SPECTROSCOPY SURVEYS: OXYGEN ABUNDANCE GRADIENTS

S. F. Sánchez¹ and L. Sánchez-Menguiano²

RESUMEN

Mostramos aquí los resultados recientes en los estudios del gradiente de abundancia de oxígeno mediante el uso de Espectroscopía de campo integral. En particular hemos analizado 2124 cubos de datos correspondientes a objetos individuales observados por CALIFA (~ 734 objetos) y la muestra pública de MaNGA (~ 1389 objetos), derivando el gradiente de la abundancia oxígeno para cada galaxia individual. Confirmamos resultados anteriores que muestran que la forma del gradiente es muy similar para todas las galaxias con masa por encima de $10^{9.5}M_{\odot}$, presentando en media una pendiente muy parecida de $\sim -0.04\text{dex}$ dentro del rango de distancias entre $0.5\text{--}2.0 r_e$, con una posible caída en las zonas centrales ($r < 0.5r_e$) y un aplanamiento en las externas. Para masas más pequeñas el gradiente tiende a ser mas plano que para las galaxias más masivas. Todos estos resultados están de acuerdo con un crecimiento de dentro hacia fuera en las galaxias masivas y parecen indicar que las menos masivas aun están en la fase de crecimiento de fuera hacia dentro.

ABSTRACT

We present here the recent results on our understanding of oxygen abundance gradients derived using Integral Field Spectroscopic surveys. In particular we analyzed more than 2124 datacubes corresponding to individual objects observed by the CALIFA (~ 734 objects) and the public data by MaNGA (~ 1390 objects), deriving the oxygen abundance gradient for each galaxy. We confirm previous results that indicate that the shape of this gradient is very similar for all galaxies with masses above $10^{9.5}M_{\odot}$, presenting in average a very similar slope of $\sim -0.04\text{dex}$ within $0.5\text{--}2.0 r_e$, with a possible drop in the inner regions ($r < 0.5r_e$) and a flattening in the outer regions. For lower masses ($>10^{9.5}M_{\odot}$) the gradient seems to be flatter than for more massive ones. All these results agree with an inside-out growth of massive galaxies and indicate that low mass ones may still be growing in an outside in phase.

Key Words: H II regions — galaxies: general — galaxies: evolution — galaxies: ISM

1. GENERAL

It is well known that spiral galaxies present radial gradients in many of their properties, including their luminosity, colors (e.g. Searle et al. 1973), stellar and gas mass densities, ages and metallicities of their stellar populations (e.g. Sánchez-Blázquez & et al. 2014; Sánchez-Blázquez & et al. 2014; González Delgado & et al. 2015), and the abundances in different elements (e.g. Pérez-Montero & et al. 2016). In particular, spiral galaxies are known to exhibit oxygen abundance gradients since the last four decades (e.g. Peimbert et al. 1977; Alloin & et al. 1979). This result seems to indicate that disk grows inside-out, with a relatively quick self enrichment with oxygen and an almost universal negative metallicity gradient once it is normalized to the galaxy optical size (e.g.

Boissier & Prantzos 2000). This was already evident in early works (e.g. Lacey & Fall 1985; Guesten & Mezger 1982; Clayton 1987), where numerical models explain this radial gradient by combining the effects of a star-formation rate and a gas infall, that changes along the galactocentric distance (e.g., Mollá & Roy 1999).

However, the exact parametrization of the different ingredients that conform the oxygen abundance gradient in disk galaxies are not fully constrained. Oxygen abundance gradients have been studied in the last two decades by many different authors that targeted mostly individual HII regions in somehow nearby galaxies (e.g. Diaz 1989; Vila-Costas & Edmunds 1992; Zaritsky et al. 1994; Martin & Roy 1994; Bresolin et al. 2005; Bresolin 2007; Bresolin et al. 2012; Rosales-Ortega & et al. 2012, , for citing just a few). Almost all these studies seem to indicate that Milky-Way-like galaxies present a shallow negative abundance gradient, that seems to be rather uniform when normalized to a characteristic

¹Instituto de Astronomía, Universidad Nacional Autónoma de México, A.P. 70-264, 04510 México, D.F., Mexico (sfsanchez@astro.unam.mx).

²Instituto de Astrofísica de Andalucía (CSIC), Glorieta de la Astronomía s/n, Aptdo. 3004, 18080 Granada, Spain.

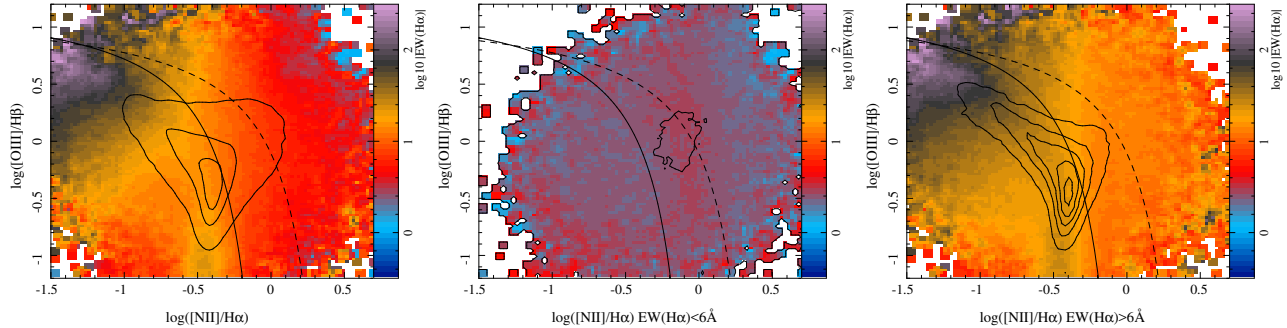


Fig. 1. $[\text{O III}] \lambda 5007/\text{H}\beta$ vs. $[\text{N II}] \lambda 6583/\text{H}\alpha$ diagnostic diagram for the $\sim 1.7\text{M}$ ionized regions/spaxels with ionized gas detected ($> 3\sigma$) in the 734 galaxies of the final CALIFA sample. The contours show the density distribution of these regions with the diagram plane, with the outermost contour enclosing 95% of the regions, and each consecutive one enclosing 20% less regions. The color indicates the logarithm of the absolute value of the $\text{EW}(\text{H}\alpha)$. *Central panel:* Same diagnostic diagram, restricted to those ionized regions with $\|\text{EW}(\text{H}\alpha)\| < 6\text{\AA}$ ($\sim 500,000$ spaxels). *Right panel:* Same diagnostic diagram, restricted to those ionized regions with $\|\text{EW}(\text{H}\alpha)\| > 6\text{\AA}$ ($\sim 1,200,000$ spaxels). In all the panels, the solid and dashed lines represent the so-called Kauffmann and Kewley demarcation curves, respectively.

scale length of the galaxy. On the other hand it is known that low mass/dwarf galaxies present an homogeneous abundance distribution (e.g. Kehrig et al. 2008), what may indicate that there is a lower-mass threshold for the inside-out growth in galaxies (e.g. Ibarra-Medel et al. 2016).

However, in most of the cases the analyzed galaxies were not selected in a systematic way, what may hamper some of the results. The advent of Integral Field Spectroscopic (IFS) surveys of galaxies like CALIFA (Sánchez & et al. 2012b), MaNGA (Bundy & et al. 2015) and SAMI (Croom et al. 2012) have overcome that problem. Observing well defined samples of galaxies, representative of the population in the nearby or Local Universe, covering the full optical extension up to $1.5r_e$ (or even beyond), these surveys allow to study the oxygen abundance gradients in a systematic way either selecting individual Hii regions (e.g. Sánchez & et al. 2012a, 2014), or regions ionized by star-formation (e.g. Sánchez-Menguiano & et al. 2016b; Zinchenko et al. 2016). In general they have found that the oxygen abundance gradient presents a common slope of $\alpha_{\text{O}/\text{H}} \sim -0.05$ dex to ~ -0.15 dex (depending on the calibrator), for galaxies more massive than $10^{9.5}\text{M}_\odot$.

In this review we present the more recent results on oxygen abundance gradient derived using IFS data extracted from the CALIFA and MaNGA surveys, summarizing the implications of these results.

2. DATA AND ANALYSIS

The results presented here correspond to the analysis performed over two different dataset. The final sample of galaxies observed by CALIFA, comprising 734 objects, and the public distribution of

galaxies observed by MaNGA, comprising 1390 objects, included in the SDSS DR13 (SDSS Collaboration et al. 2016). We analyze the datacubes using the PIPE3D pipeline (Sánchez & et al. 2016b), which is designed to fit the continuum with stellar population models and measure the nebular emission lines of IFS data. This pipeline is based on the FIT3D fitting package (Sánchez & et al. 2016a).

First the stellar population is modeled with a library of single stellar populations (SSPs) for each spaxel within the cube. This SSP model allows us to derive the stellar mass density and the integrated stellar mass (e.g. Barrera-Ballesteros & et al. 2016). Then, this model is subtracted to the original cube to create a gas-pure cube comprising only the ionised gas emission lines (and the noise). Individual emission line fluxes were then measured spaxel by spaxel using both a single Gaussian fitting for each emission line and spectrum, and a weighted momentum analysis, as described in Sánchez & et al. (2016b). For this particular dataset we extracted the flux intensity of the following emission lines: $\text{H}\alpha$, $\text{H}\beta$, $[\text{O II}] \lambda 3727$, $[\text{O III}] \lambda 4959$, $[\text{O III}] \lambda 5007$, $[\text{N II}] \lambda 6548$, $[\text{N II}] \lambda 6583$, $[\text{S II}] \lambda 6717$ and $[\text{S II}] \lambda 6731$. The intensity maps for each of these lines are corrected by dust attenuation, derived using the spaxel-to-spaxel $\text{H}\alpha/\text{H}\beta$ ratio. Then it is assumed a canonical value of 2.86 for this ratio (Osterbrock 1989), and adopting a Cardelli et al. (1989) extinction law and $R_V=3.1$ (i.e., a Milky-Way like extinction law).

To derive the oxygen abundance we select only those spaxels which ionization is compatible with being produced by star-forming areas following

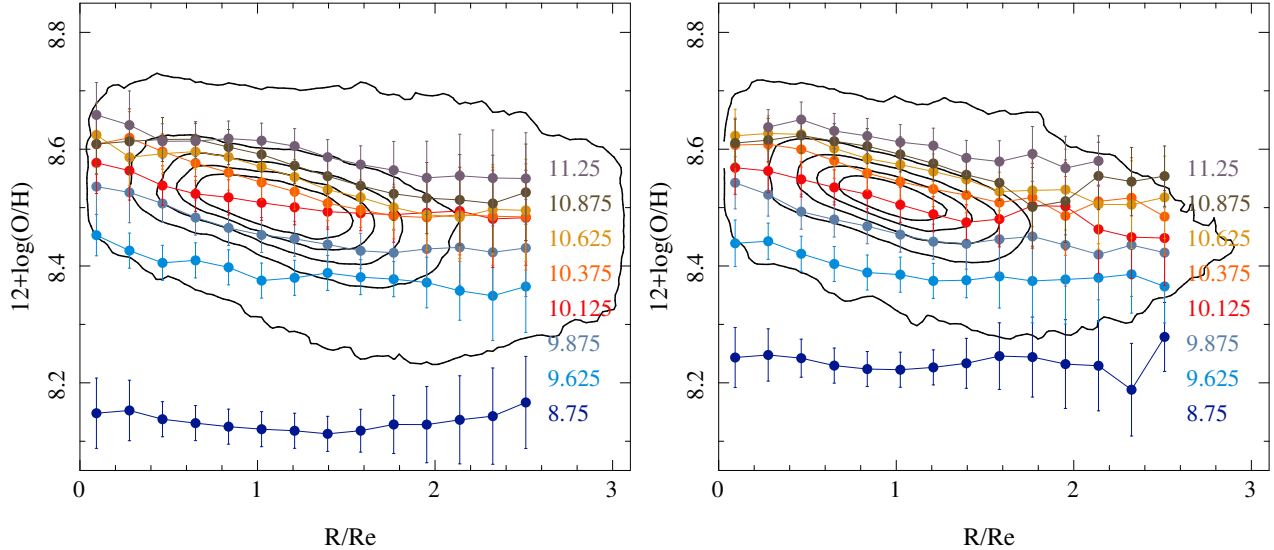


Fig. 2. Average oxygen abundance gradients derived for galaxies at different mass bins extracted from the CALIFA (left panel) and MaNGA (right panel) IFU surveys. Each solid-line of different color corresponds to one particular mass bin, with the average value labeled in the figure. Errorbars indicate the standard deviation of the distribution of abundance gradients for each bin. The contours show the density distribution of the abundances when normalized by the expected value corresponding to the Mass-Metallicity relation. Like in the previous figure the outermost contour enclosing 95% of the regions, and each consecutive one enclosing 20% less regions.

Sánchez & et al. (2013). For doing so we select those spaxel located below the Kewley et al. (2001) demarcation curve in the classical BPT diagnostic diagram (Baldwin & et al. 1981, $[\text{O III}]/\text{H}\beta$ vs $[\text{N II}]/\text{H}\alpha$ diagram.), and with a $\text{EW}(\text{H}\alpha)$ larger than 6 \AA . This criteria ensures that the ionization is compatible with being due to young stars (Sánchez & et al. 2014). Figure 1 illustrates the selection process, showing the distribution of ionized regions across the classical BPT diagram segregated by the $\text{EW}(\text{H}\alpha)$. It highlights the fact that the diffuse ionized gas, most probably related with ionization due to old stars, is covering an area that expands from the classical location of Hii regions to the area of LI(N)ER-like ionization (e.g Binette et al. 2009; Sarzi & et al. 2010; Singh & et al. 2013; Belfiore & et al. 2017). For this particular analysis we adopted the O3N2 calibrator proposed by Marino & et al. (2013). As already shown in Sánchez-Menguiano & et al. (2016b) the quantitative measurement of the oxygen abundance gradient depends on the adopted calibrator. However, the qualitative results, both regarding the shape and the distribution for different masses are all consistent.

3. RESULTS AND CONCLUSIONS

Figure 2 shows the radial abundance gradient for different stellar mass bins derived by deproject-

ing the bidimensional individual abundance distributions and obtaining azimuthal average values for all the galaxies within the considered bin. The mass bins span from $\sim 10^{8-9}M_{\odot}$ to $\sim 10^{11.0-11.5}M_{\odot}$, and were selected to have a minimum of number of ~ 30 galaxies per bin and cover the mass distribution in the most homogenous way. The analysis was repeated for both datasets, that are shown in separate panels. In both cases it is appreciated that the oxygen abundance gradients have a very similar slope above $> 10^9M_{\odot}$ in the range between $0.5-2.0 r_e$ as already shown many authors (e.g. Sánchez & et al. 2012a, 2014; Sánchez-Menguiano & et al. 2016b). For this particular calibrator the slope of this characteristic abundance gradient is of the order of $\alpha_{\text{O/H}} \sim -0.04$ dex for both datasets, with a large dispersion ($\sigma_{\alpha} \sim 0.05$ dex). Below that stellar mass, and in the case of MaNGA, below $< 10^{9.75}M_{\odot}$, the abundance gradient is shallower. This result has recently been confirmed in a detailed study presented by Belfiore et al. (submitted), using the full MaNGA dataset.

This is more clearly appreciated in Figure 3, where it is shown the distribution of individual slopes along the stellar mass for the two datasets. The mean slope for the abundance gradient is very stable within the mass range between $10^{9.5}$ and $10^{11.5}M_{\odot}$, which a large dispersion. On the other hand, for

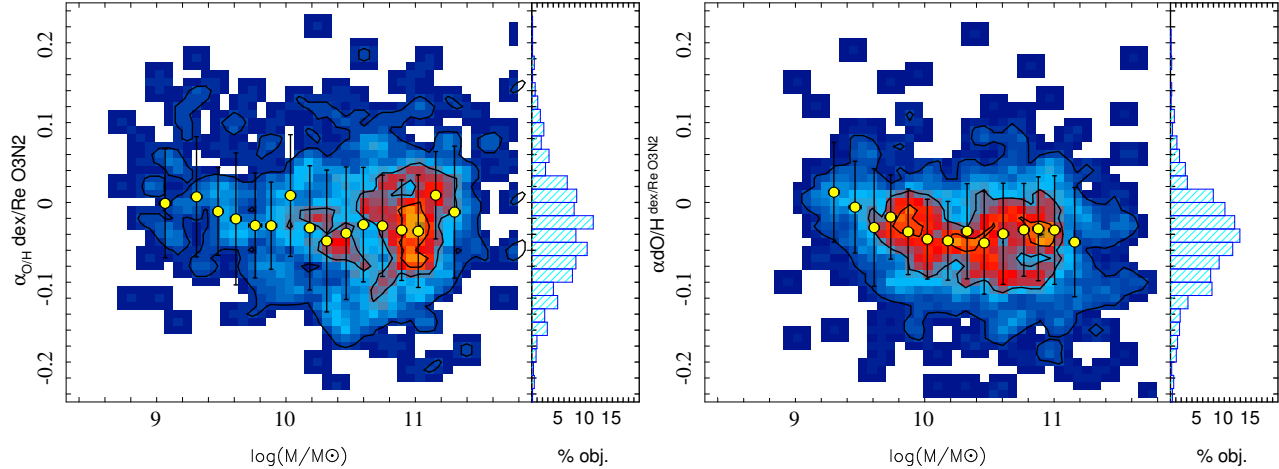


Fig. 3. Distribution of the slopes ($\alpha_{O/H}$) of the individual oxygen abundance gradients derived for each galaxy along the stellar masses for the CALIFA (left panel) and MaNGA (right panel) IFU surveys. The contours show the density distribution of the individual values. Like in the previous figure the outermost contour enclosing 95% of the regions, and each consecutive one enclosing 20% less regions. Yellow circles indicate the average value at each mass, and the error bars indicate the standard deviation, with in bins of 0.2 dex in stellar masses.

low stellar masses ($<10^{9.5}M_{\odot}$) the slope tends to zero (i.e., the absence of a gradient).

Regarding the shape of the oxygen abundance, like it was described in Sánchez-Menguiano & et al. (2016b), in addition to the negative gradient there are two additional features: (1) a flattening in the outer regions, beyond $2r_e$, visible at any mass range, and (2) a drop in the inner regions ($r < 0.5r_e$), that it is more evidence in the more massive galaxies. While the common negative gradient is interpreted as an evidence of the inside-out chemical enrichment of the galaxies, the two additional features have a less evident explanation. For the flattening in the outerpart is invoked a set of possible explanations, including radial migrations, a change in the star-formation efficiency, or a connection with stellar profile breaks (e.g. Marino & et al. 2016). The drop in the inner part could be due to the effects of strong outflows and the reach of an *equilibrium* oxygen abundance, as proposed by Belfiore et al. (2016), or the half of metal enrichment due to the quenching of star-formation associated with the bulge (e.g. Sánchez-Menguiano & et al. 2016b).

In general these results, already hinted in historical analysis based on single galaxies (or limited samples), indicate that disk galaxies present a inside-out chemical enrichment growth for stellar masses above $>10^9M_{\odot}$, while below that limit the chemical enrichment is more homogeneous. We should note that this change of behavior happens at the stellar mass at which the mass assembly transits from an inside-out and homogeneous growth (for the more

massive galaxies), to an almost outside-in and heterogeneous growth (for the less massive ones), as shown by Ibarra-Medel et al. (2016). The existence of an abundance gradient has been recently connected with the existence of a stellar-mass density relation with the local oxygen abundance, i.e., the so called Σ_*Z relation (Rosales-Ortega & et al. 2012), what has been explored by Barrera-Ballesteros & et al. (2016). These two results indicate that local stellar-mass growth and metal enrichment are two connected processes that happen in a local way, shaping the disk of galaxies, and limiting the roles of galactic outflows and radial migration as evolution drivers in this kind of galaxies.

We should conclude indicating that while current IFS surveys seem to converge in their conclusions they still present some problems to address the detailed study of oxygen abundance gradients. The most important one is the limited spatial resolution. In the case of CALIFA, MaNGA and SAMI, they three have a projected spatial resolution of $FWHM \sim 2.5''$. However, due to the very different redshift range covered by the three of them, this is translated to a very different physical scale (from $\sim 1\text{kpc}$ in the first case, to $\sim 4\text{ kpc}$ in the last one). Mast & et al. (2014) already illustrated how the abundance gradients may be affected by the lack of resolution. This issue was recently addressed by Zhang & et al. (2016), indicating how the diffuse affects the line ratios for starforming regions. For that reasons the advent of new wide-field and direct-image like spatial resolution IFUs, like MUSE (Bacon & et al.

2010), may open new possibilities of exploration of this topic, as has been already demonstrated by recent studies (e.g. Sánchez & et al. 2015; Sánchez-Menguiano & et al. 2016a).

SFS thanks the CONACYT-125180, DGAPA-IA100815 and DGAPA-IA101217 projects for providing him support in this study.

This study uses data provided by the Calar Alto Legacy Integral Field Area (CALIFA) survey (<http://califa.caha.es/>), and the MaNGA survey (SDSS-IV).

Funding for the Sloan Digital Sky Survey IV has been provided by the Alfred P. Sloan Foundation, the U.S. Department of Energy Office of Science, and the Participating Institutions. SDSS-IV acknowledges support and resources from the Center for High-Performance Computing at the University of Utah. The SDSS web site is www.sdss.org.

REFERENCES

- Alloin, D. & et al. 1979, *A&A*, 78, 200
- Bacon, R. & et al. 2010, in *SPIE Conf. Series*, Vol. 7735
- Baldwin, J. A. & et al. 1981, *PASP*, 93, 5
- Barrera-Ballesteros & et al. 2016, *MNRAS*, 463, 2513
- Belfiore, F. & et al. 2017, *MNRAS*, 466, 2570
- Belfiore, F., Maiolino, R., & Bothwell, M. 2016, *MNRAS*, 455, 1218
- Binette, L., Flores-Fajardo, N., Raga, A. C., Drissen, L., & Morisset, C. 2009, *ApJ*, 695, 552
- Boissier, S. & Prantzos, N. 2000, *MNRAS*, 312, 398
- Bresolin, F. 2007, *ApJ*, 656, 186
- Bresolin, F., Kennicutt, R. C., & Ryan-Weber, E. 2012, *ArXiv e-prints*
- Bresolin, F., Schaerer, D., González Delgado, R. M., & Stasińska, G. 2005, *A&A*, 441, 981
- Bundy, K. & et al. 2015, *ApJ*, 798, 7
- Cardelli, J. A., Clayton, G. C., & Mathis, J. S. 1989, *ApJ*, 345, 245
- Clayton, D. D. 1987, *ApJ*, 315, 451
- Croom, S. M., , & et al. 2012, *MNRAS*, 421, 872
- Diaz, A. I. 1989, in *Evolutionary Phenomena in Galaxies*, ed. J. E. Beckman & B. E. J. Pagel, 377–397
- González Delgado, R. M. & et al. 2015, *ArXiv e-prints*
- Guesten, R. & Mezger, P. G. 1982, *Vistas in Astronomy*, 26, 159
- Ibarra-Medel, H. J., Sánchez, S. F., & et al. 2016, *MNRAS*, 463, 2799
- Kehrig, C., Vílchez, J. M., Sánchez, S. F., Telles, E., Pérez-Montero, E., & Martín-Gordón, D. 2008, *A&A*, 477, 813
- Kewley, L. J., Dopita, M. A., Sutherland, R. S., Heisler, C. A., & Trevena, J. 2001, *ApJ*, 556, 121
- Lacey, C. G. & Fall, S. M. 1985, *ApJ*, 290, 154
- Marino, R. A. & et al. 2013, *A&A*, 559, A114
- _____. 2016, *A&A*, 585, A47
- Martin, P. & Roy, J.-R. 1994, *ApJ*, 424, 599
- Mast, D. & et al. 2014, *A&A*, 561, A129
- Mollá, M. & Roy, J.-R. 1999, *ApJ*, 514, 781
- Osterbrock, D. E. 1989, *Astrophysics of gaseous nebulae and active galactic nuclei* (University Science Books)
- Peimbert, M., Torres-Peimbert, S., & Rayo, J. F. 1977, in *BAAS*, 9, 302
- Pérez-Montero, E. & et al. 2016, *A&A*, 595, A62
- Rosales-Ortega, F. F. & et al. 2012, *ApJ*, 756, L31
- Sánchez, S. F. & et al. 2012a, *A&A*, 538, A8
- _____. 2012b, *A&A*, 546, A2
- _____. 2013, *A&A*, 554, A58
- _____. 2014, *A&A*, 563, A49
- _____. 2015, *A&A*, 573, A105
- _____. 2016a, *RevMexA&A*, 52, 21
- _____. 2016b, *RevMexA&A*, 52, 171
- Sánchez-Blázquez, P. & et al. 2014, *MNRAS*
- Sánchez-Blázquez, P. & et al. 2014, *ArXiv e-prints*
- Sánchez-Menguiano, L. & et al. 2016a, *ApJ*, 830, L40
- _____. 2016b, *A&A*, 587, A70
- Sarzi, M. & et al. 2010, *MNRAS*, 402, 2187
- SDSS Collaboration, Albareti, F. D., & et al. 2016, *ArXiv e-prints*
- Searle, L., Sargent, W. L. W., & Bagnuolo, W. G. 1973, *ApJ*, 179, 427
- Singh, R. & et al. 2013, *A&A*, 558, A43
- Vila-Costas, M. B. & Edmunds, M. G. 1992, *MNRAS*, 259, 121
- Zaritsky, D., Kennicutt, Jr., R. C., & Huchra, J. P. 1994, *ApJ*, 420, 87
- Zhang, K. & et al. 2016, *ArXiv e-prints*
- Zinchenko, I. A., Pilyugin, L. S., Grebel, E. K., Sánchez, S. F., & Vílchez, J. M. 2016, *MNRAS*, 462, 2715